MATERIALS CHEMISTRY FRONTIERS

CCS 中国化学会 CHINESE CHEMICAL SOCIETY

ICCAS

ROYAL SOCIETY OF CHEMISTRY

RESEARCH ARTICLE

View Article Online
View Journal | View Issue

Check for updates

Cite this: *Mater. Chem. Front.*, 2022, **6**, 948

A photoactive Ir–Pd bimetallic cage with high singlet oxygen yield for efficient one/two-photon activated photodynamic therapy†

Yuan-Yuan Liu,‡[a] Hui-Juan Yu,‡[b] Ya-Ping Wang,[a] Chao-Jie Li,[a] Xiao-Fei Wang,[b] Cai-Guo Ye,[b] Hong-Liang Yao,[b] Mei Pan *[a] and Cheng-Yong Su *[a]

Received 3rd December 2021,
Accepted 21st February 2022

DOI: 10.1039/d1qm01578h

rsc.li/frontiers-materials

Published on 24 2022. Downloaded on 15-11-2024 19:43:12.

Photodynamic therapy (PDT) has been extensively studied as a noninvasive treatment option; however, the current PDT agents are often restricted with poor solubility, difficult accumulation in tumor sites, low singlet oxygen yield and low penetration depth. Herein we develop a one-/two-photon excitation $[Pd_4Ir_8]^{16+}$ supramolecular cage (MOC-53) comprising multiple Ir(III) metalloligands, which can be quickly taken up by cancer cells to locate in the mitochondria with an ultra-high singlet oxygen generation efficiency (0.84). In particular, MOC-53 also exhibits singlet oxygen generation capability under two-photon excitation to enhance the depth of penetration and reduce photo-damage. JC-1 assays, Annexin V-FITC/PI assays and the activity of caspase-3/7 analyses show that MOC-53 can activate apoptosis efficiently. The tumor volume growth of mice after the intra-tumoral injection of MOC-53 is obviously restrained under the two-photon irradiation, showing a potential opportunity for photodynamic cancer treatment.

1. Introduction

Photodynamic therapy (PDT), in which photosensitizers (PS) convert oxygen into cytotoxic ROS (reactive oxygen species, such as singlet oxygen, $^1O_2$) and ultimately enable the destruction of cancer cells under light irradiation with specific wavelengths,[1–3] has become an emerging strategy for cancer therapy with obvious therapeutic efficiency and low side effects.[4] To date, most of the known PDT agents have suffered from poor water solubility,[5] difficult accumulation in tumor sites,[2] low chemical stability[6] and so on. In addition, ROS, especially $^1O_2$, are susceptible to the drawbacks of a short lifespan and very limited active radius, thus limiting the delivery of ROS to the desired regions such as mitochondria which are recognized as the preferential subcellular target for phototherapy before fast decay and degradation.[2,7–11] On the other hand, the two-photon photodynamic therapy utilizing low-energy light (700–950 nm) can overcome the problem of low penetration depth of one-photon photodynamic therapy to reduce the photo-damage.[12,13] Therefore, the development of an ideal photosensitizer with good two-photon absorption (TPA) which not only can target mitochondria but also have a high $^1O_2$ yield resulting in cell apoptosis is of urgent need to improve the efficacy of photodynamic therapy.[14] Metal–organic cages (MOCs), as one class of molecular containers and devices, have attracted a lot of interests in biomedical application including drug delivery, bio-imaging, cancer therapy and so on. Owing to a heavy-atom effect, iridium can facilitate efficient intersystem crossing (ISC) from the singlet excited state (S_1) or the ground state (S_0) to the triplet excited state (T_1) resulting in high yields of $^1O_2$ generation for the enhancement of PDT.[15] Ir(III)-containing MOCs assembled from multiple Ir-metalloligands have been found to not only possess superior phosphorescence properties such as large Stokes shifts, long lifetime, and high photostability,[12,14] but also have favorably enhanced permeability and retention effects in comparison with simple Ir-complexes,[16] owing to their larger size and cooperative activity derived from well-organized functional components. Moreover, Ir(III)-containing MOCs can validly overcome the disadvantages of Ir-complexes with poor insolubility in aqueous media.[17] Nevertheless, up to now, MOCs comprising Ir(III) units for accurate targeting in subcellular organelles have been barely explored.[14,18]

Herein we present a new photoactive $[Pd_4Ir_8]^{16+}$ cage (MOC-53), in which 8 Ir(III)-based PSs and 4 Pd-based acceptors are combined in a highly ordered cubic cage, acting as an efficient mitochondria-targeting one-photon and two-photon PDT agent

[a] *MOE Laboratory of Bioinorganic and Synthetic Chemistry, Lehn Institute of Functional Materials, School of Chemistry, Sun Yat-Sen University, Guangzhou 510275, China*

[b] *Guangdong Key Laboratory of Animal Conservation and Resource Utilization, Guangdong Public Laboratory of Wild Animal Conservation and Utilization, Institute of Zoology, Guangdong Academy of Sciences, Guangzhou 510260, China. E-mail: panm@mail.sysu.edu.cn, cesscy@mail.sysu.edu.cn*

† Electronic supplementary information (ESI) available. See DOI: 10.1039/d1qm01578h

‡ These authors contributed equally.

 This journal is © The Royal Society of Chemistry and the Chinese Chemical Society 2022

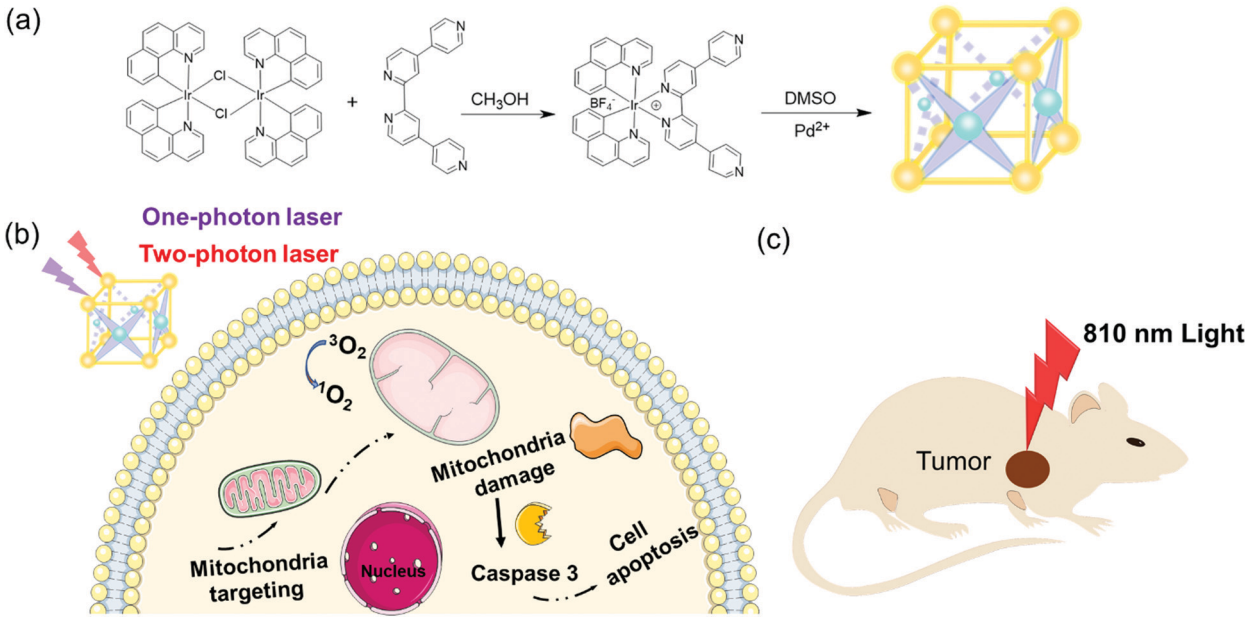

Scheme 1 (a) Synthesis of Irqpy-2 metalloligand and MOC-53. (b and c) Schematic of the PDT effect of MOC-53 toward a tumor-bearing mouse with 810 nm light irritation.

Published on 24 2022. Downloaded on 15-11-2024 19:43:12.

to take advantage of both Ir-complexes and cage integrity (Scheme 1). MOC-53 displays appropriate water solubility, higher $^1O_2$ generation efficiency upon irradiation, favorable cellular uptake, and specific mitochondria-targeting ability, causing effective cell death in cancer cells. We have studied the death mechanism in the PDT process by assaying the disruption of the mitochondrial membrane and activity of Annexin V-FITC/PI and the caspase-3/7 proteins in HeLa cells. We also demonstrate the significant anti-tumor efficacy of two-photon PDT by *in vivo* studies on CT-26 tumor-bearing mice. The results confirm that heterometallic MOC-53 has a highly excellent one-photon and two-photon therapeutic effect.

2. Experimental

2.1 Materials and instrument

All reagents of analytical grade were purchased commercially and used without further purification. ^{1}H NMR data were obtained using a Bruker AVANCE III (400 MHz) in DMSO-d_6 or $CDCl_3$ solution. The luminescence (excitation and emission) spectra of the samples were recorded using an Edinburgh FLS 980 PL spectrometer. The absolute photoluminescence quantum yields (PLQYs) were measured on a Hamamatsu C9920-02G system. The UV-Vis absorption data were obtained using a SHIMADZU UV-3600 equipped with an integrating sphere using BaSO4 as a reference. The HR-MS spectra were recorded on Bruker maXis 4G ESI-Q-TOF equipment. The data of ESI-TOF mass spectrometry were analyzed using Bruker Data Analysis software and simulated using Bruker Isotope Pattern software.

2.2 Synthesis

4,4′:2′,2″:4″,4‴-quaterpyridine (qpy). The ligand qpy was acquired as previously reported. ^{1}H NMR (400 MHz, $CDCl_3$) δ 8.83 (d, 2H, J = 5.0 Hz), 8.78 (d, 6H, J = 6.2 Hz), 7.69 (d, 4H, J = 6.0 Hz), 7.61 (d, 2H, J = 5.0 Hz).

Synthesis of $[Ir(bzq)_2(\mu\text{-}Cl)]_2$. $IrCl_3{\cdot}3H_2O$ (1.208 g, 3.4 mmol) and benzquinamide (bzq, 1.147 g, 4 mmol) were added to a mixture of 60 mL ethylene glycol ether/water (v : v = 3 : 1). The mixed solution was heated and stirred at 120 °C to reflux overnight under a nitrogen atmosphere. Then 20 mL deionized water was added into the mixed solution to adjust the polarity after cooling to room temperature. A large amount of yellow solid was precipitated from the solution, which was washed with ethanol and ether and dried under vacuum. Without tedious purification, $[Ir(bzq)_2(\mu\text{-}Cl)]_2$ was directly used to synthesize the next step of the metalloligand.

$[Ir(bzq)_2(qpy)]{\cdot}(BF_4)$ (Irqpy-2). $[Ir(bzq)_2(\mu\text{-}Cl)]_2$ (113 mg, 0.18 mmol) and 4,4′:2′,2″:4″,4‴-quaterpyridine (qpy, 114 mg, 0.37 mmol) were added to a mixture of CH_2Cl_2/MeOH (v : v = 1 : 1) for 10 mL. The red solution was heated at 60 °C overnight under a nitrogen atmosphere. After cooling, 20 mL water was added and the aqueous layer was collected, which was washed with ether. After heating the solution at 75 °C, saturated $NaBF_4$ solution was added. Finally, an orange solid was obtained, which was filtered and washed with water and ether. The pure product of Irqpy-2 metalloligand was obtained as an orange powder and the yield was 20%. ^{1}H NMR (400 MHz, DMSO-d_6): δ 9.48 (s, 2H), 8.91–8.80 (m, 4H), 8.61 (d, 2H, J = 8.0 Hz), 8.19 (d, 2H, J = 7.1 Hz), 8.10–7.89 (m, 10H), 7.68–7.53 (m, 4H), 7.22 (2, 2H, J = 7.6 Hz), 6.25 (d, 2H, J = 7.2 Hz).

$[Pd_4(Irqpy\text{-}2)_8]{\cdot}(BF_4)_{16}{\cdot}$solvents (MOC-53). 10 mg $[Ir(bzq)_2(qpy)](BF_4)$ (Irqpy-2, 0.011 mol) and 3 mg $Pd(BF_4)_2(CH_3CN)_4$ (0.0075 mmol) were dissolved in 0.5 mL DMSO. The mixture was heated and stirred at 80 °C for 8 h. Then, 5 mL ethyl acetate was added after cooling and large

Published on 24 2022. Downloaded on 15-11-2024 19:43:12.

quantity of orange precipitates was obtained. This mixture was washed vigorously with ethyl acetate and dried to afford the pure material. The yield was 85%. ^{1}H NMR (400 MHz, DMSO-d_6) δ 9.65 (s, 32H), 9.16 (s, 32H), 8.59 (s, 16H), 8.29 (s, 48H), 8.01–7.96 (m, 48H), 7.91 (d, J = 11.8 Hz, 16H), 7.61–7.55 (m, 16H), 7.48 (s, 32H), 7.28 (s, 16H), 7.20 (s, 16H), 6.67 (s, 16H), 6.20 (s, 16H), 2.07 (s, 64H), 1.76 (s, 32H).

3. Results and discussion

3.1 Structural characterization

The heterometallic MOC-53 was obtained through a facile one-pot synthesis by reacting Irqpy-2 metalloligand with $Pd(BF_4)_2(CH_3CN)_4$ in dimethyl sulfoxide (DMSO) solution at 80 °C according to our previous work, and characterized by means of ^{1}H NMR (Fig. S1–S3, ESI†), solution titrations (Fig. S4, ESI†) and MS spectra. From the ^{1}H NMR titration experiment,[19] we can see that new proton signals appear to replace those of pure Irqpy-2 metalloligand along with the addition of $Pd(BF_4)_2(CH_3CN)_4$. No more proton peak change is observed when the ratio of Ir : Pd reaches 8 : 4, indicating the formation of a definite structure through the coordination driven self-assembly process between Irqpy-2 and Pd(II) ions. According to our earlier reports,[20] we conclude that a bottom-free cubic barrel-like cage (defined as MOC-53) is assembled, in which eight Irqpy-2 metalloligands occupy the vertices of a cubic barrel, linked by four Pd(II) ions *via* the qpy pendants on the metalloligands. The high-resolution electrospray ionization time-of-flight mass spectrometry (HR-ESI-TOF-MS) is used to elucidate the solution structure of MOC-53 (Fig. S5, ESI†), which displays a series of peaks carrying +6, +7 and +8 charges with m/z values of 1361.06, 1154.19 and 999.17, respectively, well matching with the simulated data of the MOC-53 cage *via* successive loss of the tetrafluoroborate ions.

3.2 Photophysical features

The photophysical properties of MOC-53 and free Irqpy-2 metalloligand in DMSO solution were investigated as presented in Fig. S6–S10 (ESI†). Attributed to the metal-to-ligand charge transfer (MLCT) and the π–π* transitions of bzq and qpy, both MOC-53 and Irqpy-2 show a broad absorption in 300–450 nm and a strong band at 260 nm in the ultraviolet region. MOC-53 shows similar emission peaks as Irqpy-2 at around 650 nm in DMSO solution with a large Stokes shift of 200 nm (Fig. 1a), offering great advantages for bioimaging because of the avoidance of self-quenching.[1] The absolute photoluminescence quantum yields of MOC-53 and Irqpy-2 are 5% and 7%, respectively. The luminescence lifetime of MOC-53 is 120 ns (Fig. S7, ESI†), indicative of a phosphorescent nature (Table S1, ESI†). The TPA cross-sections of Irqpy-2 and MOC-53 are measured from 720 to 880 nm at 10 nm intervals by using femtosecond laser pulses. As shown in Fig. 1b, MOC-53 displays the largest 2-photon cross-section of 783 GM, in comparison with that of 31 GM for Irqpy-2 under the same conditions,

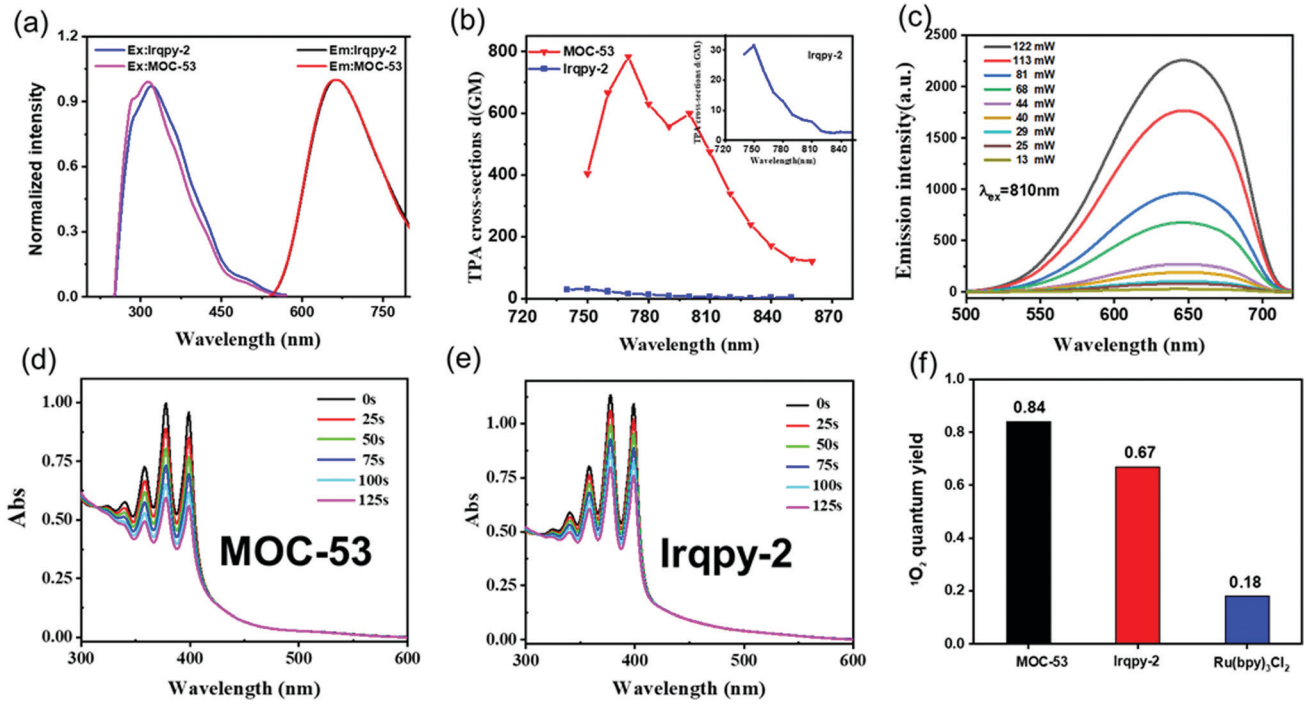

Fig. 1 (a) Normalized photoluminescent excitation (λ_{em} = 660 nm) and emission (λ_{ex} = 330 nm) spectra of MOC-53 (DMSO, 1.25 × 10^{-6} mol L^{-1}) and Irqpy-2 (DMSO, 1 × 10^{-5} mol L^{-1}); (b) TPA cross sections of MOC-53 and Irqpy-2 in DMSO (λ_{ex} = 810 nm); (c) two-photon excited fluorescence spectra of MOC-53 at different excitation power in DMSO (λ_{ex} = 810 nm). (d and e) The quantum yields for $^1O_2$ production (Φ_Δ) by detecting time-evoluted UV-Vis absorption spectra of (d) MOC-53 + ABDA, and (e) Irqpy-2 + ABDA; (f) comparison of the quantum yields for $^1O_2$ production of MOC-53, Irqpy-2 and $[Ru(bpy)_3]Cl_2$ standard in water solution.

 This journal is © The Royal Society of Chemistry and the Chinese Chemical Society 2022

Published on 24 2022. Downloaded on 15-11-2024 19:43:12.

suggesting that assembly of multiple Ir-complexes into a single cage structure can give rise to a higher 2-photon cross-section. The luminescence intensities of MOC-53 and Irqpy-2 induced by a two-photon display a dependence on the logarithmic incident power (Fig. 1c and Fig. S8, ESI†), indicating that MOC-53 possesses a 2-photon active nature which is beneficial to PDT efficiency. The photo-stability of MOC-53 and Irqpy-2 has been evaluated (Fig. S9, ESI†), confirming that MOC-53 has superior stability *n* buffer solution and cell culture medium (DMEM) at room temperature for 48 h (Fig. S10, ESI†).

3.3 Singlet oxygen ($^1O_2$) quantum yield

The singlet oxygen $^1O_2$ quantum of Irqpy-2 and MOC-53 are evaluated by using 9,10-anthracenediyl-bis-(methylene) dimalonic acid (ABDA) as the $^1O_2$ indicator and $[Ru(bpy)_3]Cl_2$ with singlet oxygen quantum yield of 0.18 in H_2O as the standard substance. Upon irradiation with 425 nm a xenon lamp, the decrease of the ABDA absorption intensity is recorded (Fig. 1d, e and Fig. S11, S12, ESI†). Notably, the reduction of ABDA absorbance in the presence of MOC-53 is more significant in comparison with the faint reduction of ABDA induced by Irqpy-2, indicating that MOC-53 is more efficient than Irqpy-2 in producing $^1O_2$ under the same conditions. The $^1O_2$ quantum yields (Φ_Δ) of Irqpy-2 and MOC-53 are calculated to be 0.67 and 0.84 (Fig. 1f), respectively, which are superior to known Ir-complexes including our previously reported MOC-51, which may be attributed to the enlargement of the conjugate plane.[21,22] Also, the eight Irqpy-2 and four Pd(II) ions are organized in a highly ordered cubic manner to improve the energy transfer efficiency by multiple but independent energy transfer and electron collection pathways. These results suggest that MOC-53 is promising as an efficient PDT photosensitizer[23] (Table S2, ESI†). We also use 3-diphenylisobenzofuran (DPBF) to evaluate the $^1O_2$ quantum of Irqpy-2 and MOC-53 through their reduction of DPBF absorption intensity (Fig. S13, ESI†), which further proves the higher $^1O_2$ quantum yield of MOC-53 than Irqpy-2.

3.4 Cellular uptake and localization

Since therapeutic efficacy is also correlated with efficient cellular uptake, we investigate the cellular uptake of MOC-53 by human cervical adenocarcinoma (HeLa) cells with confocal microscopy. Firstly, the octanol/water partition coefficients log Po/w of MOC-53 was assessed by a shake-flask method.[24] The octanol/water partition coefficient (log Po/w) of MOC-53 was calculated to be 0.1, which may be attributed to its cell uptake efficiency. The cells are cultured in a media containing 0.2, 0.6, 1 and 2 μM of MOC-53. Clear and bright fluorescence is observed in the cell treated with 2 μM of MOC-53 (Fig. S14, ESI†). Then the cells are incubated with 2 μM MOC-53 for 30, 60, 120 and 150 min. As shown in Fig. 2a, as the incubation time is extended, the red phosphorescence of MOC-53 gradually increases (Fig. 2b), which suggests that MOC-53 is highly stable and can be steadily located in cells. The fluorescence intensity of the cells stained with MOC-53 obviously decreases with the decrease of temperature from 37 °C, 25 °C to 4 °C indicating the cellular uptake of MOC-53 is energy dependent (Fig. S15, ESI†). The subcellular co-localization of MOC-53 is further determined by the commercially available mitochondrial dye Mito-Tracker Green (MTG) and the lysomal dye Lyso-Tracker Red (LTR) as depicted in Fig. 2c. It is hardly co-localized with LTR with a relative correlation coefficient of 0.31, confirming the location of MOC-53 in the mitochondria of HeLa cells with a relative correlation coefficient of 0.78 (Fig. S16, ESI†). Since cell apoptosis is easily caused by mitochondria-targeting PSs, maximizing the cell uptake of mitochondria-targeting MOC-53 is beneficial to phototherapy.

3.5 PDT activities

An ideal PS not only generates adequate ROS for the purpose of inducing cell death upon irradiation, but also minimally destroys the biological activities of cells in the absence of light stimulation.[17] Therefore, the dark cytotoxicity and PDT activities of MOC-53 and Irqpy-2 towards HeLa cells are investigated by the MTT assay after 48 h incubation with different concentrations of MOC-53 and Irqpy-2. The PDT activities are observed when exposed to an extremely small light dose of 23 mW cm^{-2} at 425 nm for 20 min. As shown in Fig. S17, (ESI†) both MOC-53 and Irqpy-2 display no apparent toxicity to the HeLa cells in the absence of light, which is crucial for a suitable photodynamic therapy. However, MOC-53 has higher photo-toxicity than Irqpy-2 under the same conditions (Fig. 3a and b). What's more, under irradiation at 425 nm (23 mW cm^{-2}), the cytotoxicity of MOC-53 significantly increases by prolonging the concentration and irradiation time. The increasing fold (the ratio between phototoxicity and dark toxicity) of MOC-53 goes up from 1 to 10 as the time prolong to 60 min, which is larger than Irqpy-2, suggesting that the PDT efficiency of MOC-53 is sensitive to the irradiation time and the better photodynamic effect of MOC-53 resulting from an appropriate molecular size, high charges on MOC-53 (+16), and good water- solubility (Fig. 3c). In contrast, cells treated with $Ru(bpy)_3Cl_2$ exhibit negligible difference in the cytotoxicity with or without the light irradiation conditions (Fig. S18, ESI†). These results imply the potential of MOC-53 as an efficient PS for PDT compared to $Ru(bpy)_3Cl_2$ and Irqpy-2 itself.

3.6 Verification of $^1O_2$ generation in HeLa cells

To evaluate the ability of MOC-53 to generate singlet oxygen *in vitro* HeLa cells under 425 nm light irradiation, 2,7-dichlorodihydrofluorescein diacetate (DCFH-DA) is employed as an intracellular ROS indicator. The intracellular ROS level could be reflected by the green-fluorescence of DCF after oxidation of non-fluorescent DCFH. HeLa cells are incubated with MOC-53 and DCFH-DA, and the confocal fluorescence images of the cells before and after irradiation are recorded. As shown in Fig. 3d, the green fluorescence of DCF is not observed in the control, while shows a time- and concentration-dependent increase as the MOC-53 dose is increased from 0.2 to 0.8 μM (Fig. S19, ESI†), indicating the generation of $^1O_2$ in HeLa cells. We also detect the ROS generation under the two-photon irradiation (800 nm, 60 mW), confirming the ability of

Published on 24 2022. Downloaded on 15-11-2024 19:43:12.

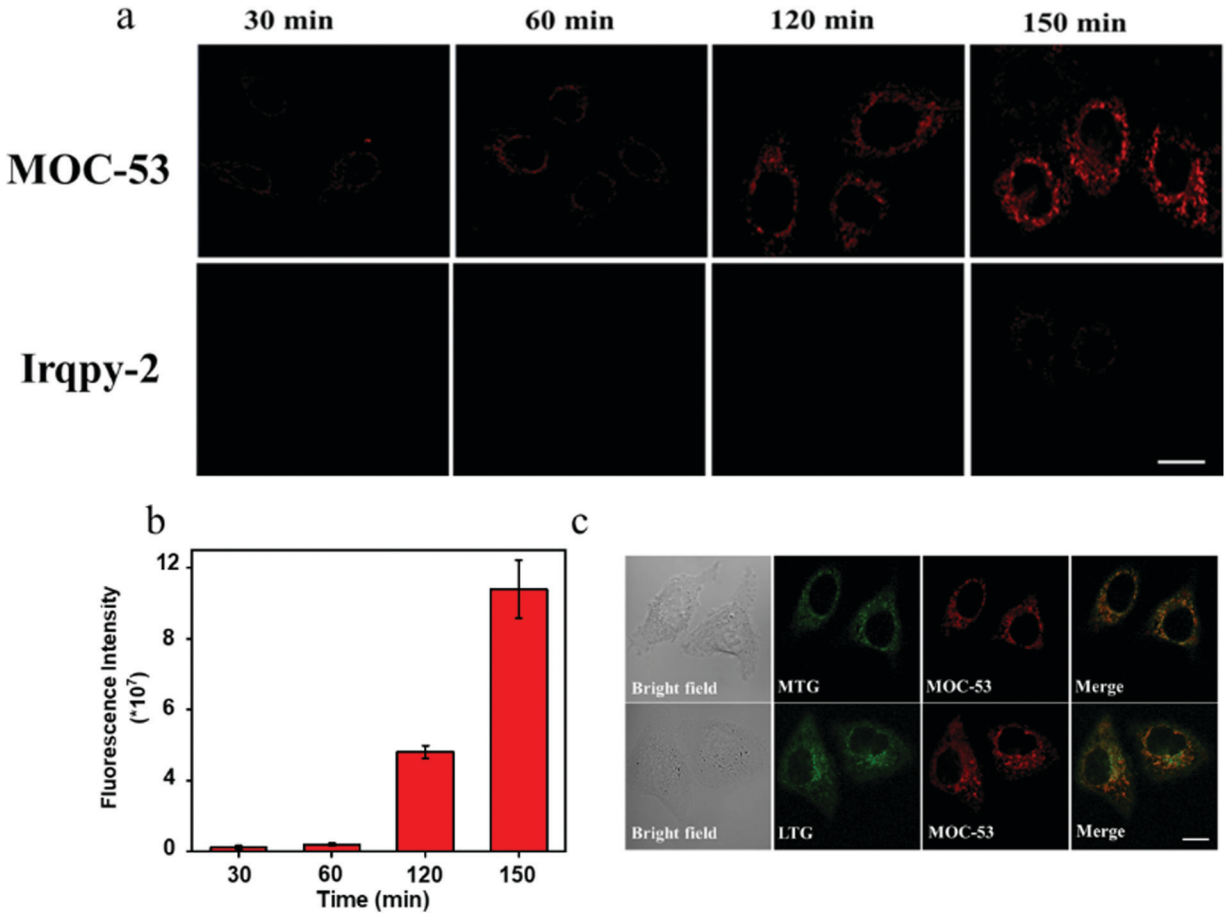

Fig. 2 (a) Confocal fluorescence images of Irqpy-2 and MOC-53 uptake in HeLa cells at 37 °C for 30, 60, 120, and 150 min, respectively. Images were captured at 650 ± 20 nm under excitation at 405 nm. Scale bar: 20 mm. (b) The fluorescence intensity of HeLa cells treated with MOC-53 (2 μM) for different time. (c) Confocal fluorescence images of HeLa cells incubated with MOC-53 (2 μM, 2 h), MTG (150 nmol L^{-1}, 30 min), and LTG (150 nmol L^{-1}, 30 min), respectively. MOC-53: λ_{ex} = 405 nm, λ_{em} = 670 ± 20 nm; MTG: λ_{ex} = 488 nm, λ_{em} = 516 ± 20 nm; LTG: λ_{ex} = 405 nm, λ_{em} = 550 ± 20 nm.

two-photon PDT of the MOC-53 at the cellular level (Fig. 3e). This observation is consistent with the concentration-dependent cellular uptake phenomenon.

3.7 Mitochondrial dysfunction

The release of proapoptotic proteins is often induced by mitochondrial dysfunction, which is regarded as a hallmark of cell apoptosis. As the mitochondrial membrane potential (MMP, $\Delta\Psi_m$) is an indicator of mitochondrial function,[25] JC-1 that forms red ''J-aggregates'' at high MMP and a green ''J-monomer'' at low MMP is used to detect the change of MMP in HeLa cells incubated with MOC-53 before and after the light irradiation (425 nm, 23 mW cm^{-2}). As shown in Fig. 4a, the cells of the control show red fluorescence while the cells treated with MOC-53 exhibit obvious green fluorescence, which indicates that the mitochondrial function is damaged by light irradiation. These results unveil that the MOC-53 can be localized in mitochondria to generate $^1O_2$ to damage the mitochondria upon irradiation, overcoming the short lifespan of the $^1O_2$ and restricting range of diffusion of the ROS to improve the PDT effect.

3.8 Cell apoptosis

The Annexin V-FITC/PI apoptosis assay kit is useful to distinguish necrotic, late apoptotic and early apoptotic cells. Therefore, we can easily differentiate the stages of apoptosis by annexin V/PI co-staining. As shown in Fig. 4b, when cells are treated with 2 μM MOC-53 under light irradiation, annexin V-FITC and PI are stained with cells, indicating late apoptosis and/or necrosis. In contrast, the control cells without irradiation are not stained with either annexin V-FITC or PI, implying that they are alive. Moreover, the annexin V-FITC and PI of HeLa cells treated with low concentrations reveal that apoptosis occurs in HeLa cells (Fig. S20, ESI†). We further evaluate the cell death mechanism.

3.9 Caspase-3/7 activity assay

The release of proapoptotic proteins is often induced by apoptosis *via* an intrinsic pathway with caspase 3/7 as key executors.[26–29] We use the Caspase-Glo assay to clarify the activation of Caspase 3/7 with the HeLa cells treated by different concentrations of MOC-53 (0.5, 1, and 2 μM) and light irradiation. As shown in Fig. 4c, treatment of MOC-53 (0.5, 1,

 This journal is © The Royal Society of Chemistry and the Chinese Chemical Society 2022

Published on 24 2022. Downloaded on 15-11-2024 19:43:12.

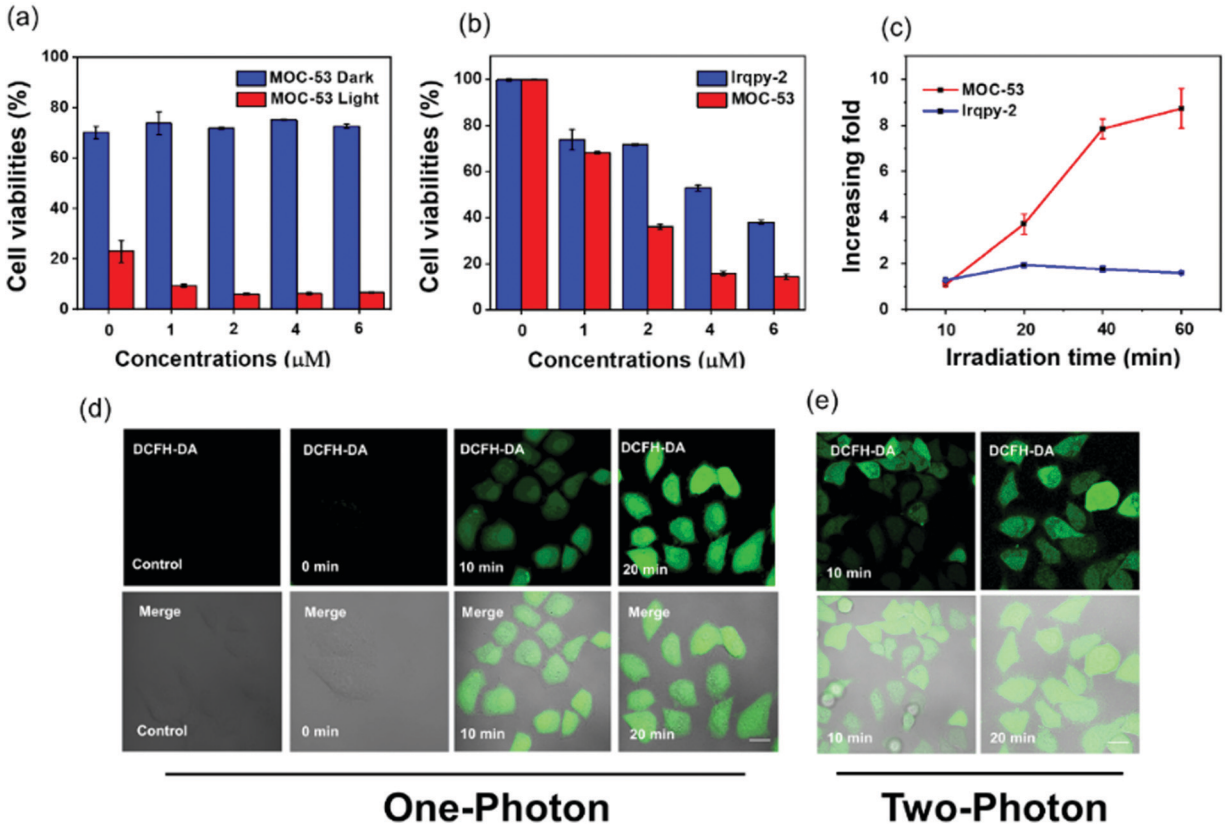

Fig. 3 (a) The cell viabilities of HeLa cells treated with different concentrations MOC-53 with or without light irradiation; (b) the photo toxicity of MOC-53 and Irqpy-2 toward HeLa cells (irradiation time: 20 min); (c) the increasing fold (the ratio of photo cytotoxicitities and dark cytotoxicities) of MOC-53 and Irqpy-2, respectively; (d and e) images of ROS generation in HeLa cells incubated with MOC-53 (2 μM, 2 h) and DCF (10 mM, 0.5 h, λ_{ex} = 488 nm, λ_{em} = 510 ± 15 nm) before and after 425 nm irradiation (23 mW cm^{-2}) and 810 nm irradiation.

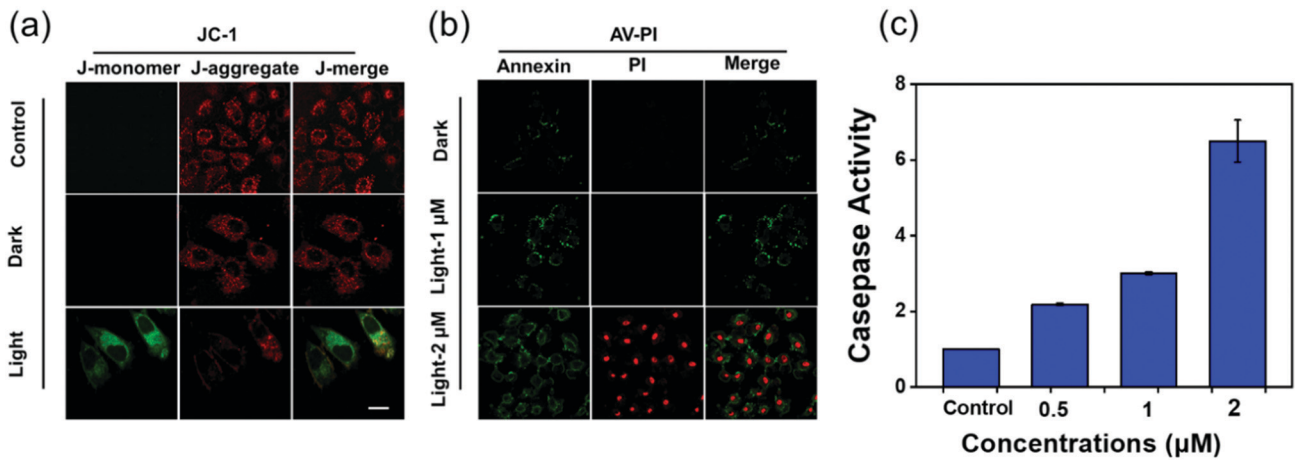

Fig. 4 (a) Confocal images of HeLa cell incubation with MOC-53 (2 μM, 2 h) and JC-1 (10 mM, 0.5 h, for the J-monomer: λ_{ex} = 488 nm, λ_{em} =510 ± 15 nm; for J-aggregates: λ_{ex} = 543 nm, λ_{em} =610 ± 20 nm) after 425 nm irradiation. Scale bars: 20 mm. (b) Confocal fluorescence images of HeLa cells incubated with MOC-53 (2 μM, 2 h) and Annexin V-FITC/PI (10 min) before and after 425 nm irradiation (23 mW cm^{-2}); Annexin V-FITC: λ_{ex} = 405 nm, λ_{em} = 670 ± 20 nm; PI: λ_{ex} = 488 nm, λ_{em} = 516 ± 20 nm; LTG: λ_{ex} = 405 nm, λ_{em} = 550 ± 20 nm; scale bars: 20 mm. (c) Caspase 3/7 activity in HeLa cells after treatment with MOC-53 (0.5, 1 or 2 μM) for 2 h after 425 nm irradiation (23 mW cm^{-2}).

and 2 μM) obviously stimulates caspase 3/7 activity after irradiation with increasing concentrations, while the control group without light irradiation shows no obvious caspase 3/7 activity. The activity of caspase 3/7 significantly increases about 2, 3 and 6-fold by adding MOC-53 with concentrations ranging from 0.5 to 2 μM, confirming that the mechanism of cell death

Published on 24 2022. Downloaded on 15-11-2024 19:43:12.

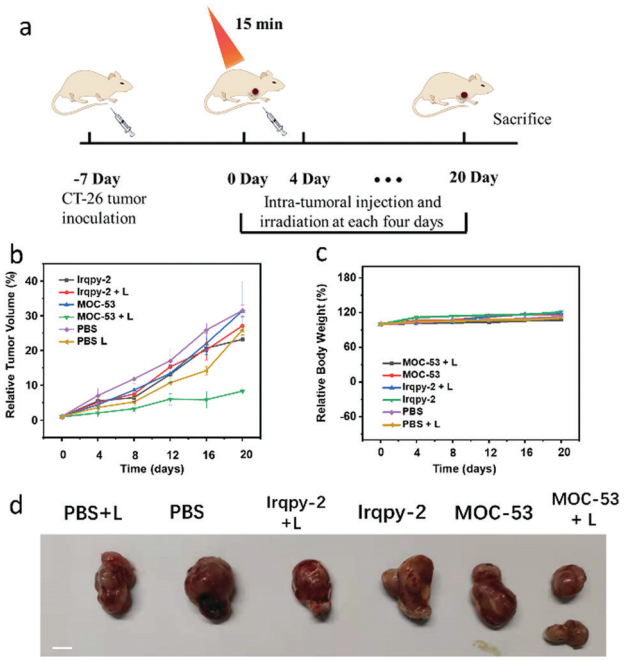

Fig. 5 (a) Therapeutic regimen of CT-26 xenograft tumor; (b) relative tu mor volume of mice after different treatments; (c) relative Body Weight of mice after different treatments; (d) images of tumors harvested in mice from different groups at 20 days of post-treatment. Scale bar: 20 mm.

is through concentration dependent apoptosis, consistent with the above mentioned results that the effectiveness of PDT is concentration-dependent.

3.10 Two-photon PDT *in vivo*

Furthermore, CT-26 tumor-bearing Balb/c mice are used to evaluate the *in vivo* two-photon PDT efficacy based on the good therapeutic effects of *in vitro* therapy (Fig. 5). After inducing the subcutaneous tumor at the forelimb axillary of mice, the tumor volume is measured every two days until its volume reaches 100–200 mm. Then, we randomly divide mice into six groups (five mice per group): (1) PBS, (2) PBS + L, (3) Irqpy-2, (4) Irqpy-2 + L, (5) MOC-53, and (6) MOC-53 + L. The groups 1–5 are treated as controls; the mice in group 1, 3, 5 are injected with PBS, Irqpy-2 and MOC-53 by intratumor injecting without light, and the mice in group 2 and group 4 are injected with PBS and Irqpy-2 (20 mg kg^{-1}) with two-photon laser irradiation (800 nm, 60 mW, 15 min), respectively. The sixth group mice are injected with MOC-53 (5 mg kg^{-1}) and treated with light equal to that of groups 2 and 4. The mice are subjected to irradiation under the same conditions used previously; the tumor volume and the body weight of mice are also measured and recorded every four days, and finally, the mice are sacrificed on day 20. As shown in Fig. 5b and d, a dramatic increase of tumor volume is observed in the control groups to show more than 20-fold growth. In contrast, injection of MOC-53 can efficaciously inhibit the tumor growth. The body weight in sixth groups, which is used to demonstrate the biosafety of MOC-53, shows no significant loss, indicating minimal side effects caused by the injection of MOC-53 and irradiation with light (Fig. 5c).

4. Conclusions

In summary, we have developed a mitochondria-targeted MOC-53 bimetallic supramolecular cage, which has bright phosphorescence and excellent photostability. Under visible light irradiation, the MOC-53 cage has an outstanding $^1O_2$ production quantum yield for PDT of up to 0.84. Importantly, the MOC-53 cage has higher light toxicity toward HeLa cells with low dark toxicity, which is a key to the effectiveness of PDT, in contrast to the Irqpy-2 complex, confirming a synergistic effect of the assembled MOCs. An evaluation of the death mechanism of HeLa cells treated with MOC-53 also supports these effects. The *in vivo* anticancer studies indicate that MOC-53 can accumulate in tumors and significantly inhibit tumor growth under two-photon irradiation, further demonstrating the excellent PDT effect and good biocompatibility of MOC-53. Therefore, the MOC-53 cage may act as an applicable agent for PDT to provide an ideal model for the development of a new class of PDT PSs, opening up an avenue for the design and creation of multi-component metal–organic materials with synergistic effects for better application in cell imaging and cancer phototherapeutics.

Conflicts of interest

There are no conflicts to declare.

Acknowledgements

This work was supported by the National Natural Science Foundation of China (21771197, 21720102007, 21821003, 21890380 and 82104228), the Local Innovative and Research Teams Project of Guangdong Pearl River Talents Program (2017BT01C161), the GDAS Special Project of Science and Technology Development (2021GDASYL–20210103057), and the High-level Leading Talent Introduction Program of Guangdong Academic of Sciences (2016GDASRC-0206). All procedures for animal experiments were strictly performed in compliance with the guideline approved by Institutional Animal Ethical and Welfare Committee of Sun Yat-Sen University.

Notes and references

1 S. Hapuarachchige, G. Montano, C. Ramesh, D. Rodriguez, L. H. Henson, C. C. Williams, S. Kadavakkollu, D. L. Johnson, C. B. Shuster and J. B. Arterburn, Design and synthesis of a new class of membrane-permeable triazaborolopyridinium fluorescent probes, *J. Am. Chem. Soc.*, 2011, **133**, 6780–6790.
2 C. Li, W. Zhang, S. Liu, X. Hu and Z. Xie, Mitochondria-Targeting Organic Nanoparticles for Enhanced Photodynamic/Photothermal Therapy, *ACS Appl. Mater. Interfaces*, 2020, **12**, 30077–30084.

 This journal is © The Royal Society of Chemistry and the Chinese Chemical Society 2022

Published on 24 2022. Downloaded on 15-11-2024 19:43:12.

3 J. Zhang, L. Ning, J. Huang, C. Zhang and K. Pu, Activatable molecular agents for cancer theranostics, *Chem. Sci.*, 2020, **11**, 618–630.
4 D. D. Wang, H. H. Wu, S. Z. F. Phua, G. B. Yang, W. Q. Lim, L. Gu, C. Qian, H. B. Wang, Z. Guo, H. Z. Chen and Y. L. Zhao, Self-assembled single-atom nanozyme for enhanced photodynamic therapy treatment of tumor, *Nat. Commun.*, 2020, **11**, 357.
5 B. Jana, A. P. Thomas, S. Kim, I. S. Lee, H. Choi, S. Jin, S. A. Park, S. K. Min, C. Kim and J. H. Ryu, Self-Assembly of Mitochondria-Targeted Photosensitizer to Increase Photostability and Photodynamic Therapeutic Efficacy in Hypoxia, *Chem. – Eur. J.*, 2020, **26**, 10695–10701.
6 X. D. Bi, R. Yang, Y. C. Zhou, D. Chen, G. K. Li, Y. X. Guo, M. F. Wang, D. Liu and F. Gao, Cyclometalated Iridium(III) Complexes as High-Sensitivity Two-Photon Excited Mitochondria Dyes and Near-Infrared Photodynamic Therapy Agents, *Inorg. Chem.*, 2020, **59**, 14920–14931.
7 W. Lv, Z. Zhang, K. Y. Zhang, H. Yang, S. Liu, A. Xu, S. Guo, Q. Zhao and W. Huang, A Mitochondria-Targeted Photosensitizer Showing Improved Photodynamic Therapy Effects Under Hypoxia, *Angew. Chem., Int. Ed.*, 2016, **55**, 9947–9951.
8 C. Zhang, F. Gao, W. Wu, W. X. Qiu, L. Zhang, R. Li, Z. N. Zhuang, W. Yu, H. Cheng and X. Z. Zhang, Enzyme-Driven Membrane-Targeted Chimeric Peptide for Enhanced Tumor Photodynamic Immunotherapy, *ACS Nano*, 2019, **13**, 11249–11262.
9 D. B. Cheng, X. H. Zhang, Y. J. Gao, L. Ji, D. Hou, Z. Wang, W. Xu, Z. Y. Qiao and H. Wang, Endogenous Reactive Oxygen Species-Triggered Morphology Transformation for Enhanced Cooperative Interaction with Mitochondria, *J. Am. Chem. Soc.*, 2019, **141**, 7235–7239.
10 X.-H. Zhang, R.-C. Guo, Y.-F. Chen, X. Xu, Z.-X. Yang, D.-B. Cheng, H. Chen, Z.-Y. Qiao and H. Wang, A BiOCl nanodevice for pancreatic tumor imaging and mitochondria-targeted therapy, *Nano Today*, 2021, 40.
11 X. Li, H. Xiao, W. Xiu, K. Yang, Y. Zhang, L. Yuwen, D. Yang, L. Weng and L. Wang, Mitochondria-Targeting MoS2-Based Nanoagents for Enhanced NIR-II Photothermal-Chemodynamic Synergistic Oncotherapy, *ACS Appl. Mater. Interfaces*, 2021, **13**, 55928–55938.
12 B. Gu, W. Wu, G. Xu, G. Feng, F. Yin, P. H. J. Chong, J. Qu, K. T. Yong and B. Liu, Precise Two-Photon Photodynamic Therapy using an Efficient Photosensitizer with Aggregation-Induced Emission Characteristics, *Adv. Mater.*, 2017, **29**, 1701076.
13 V. Juvekar, C. S. Lim, D. J. Lee, S. J. Park, G. O. Song, H. Kang and H. M. Kim, An azo dye for photodynamic therapy that is activated selectively by two-photon excitation, *Chem. Sci.*, 2021, **12**, 427–434.
14 H. Sepehrpour, W. Fu, Y. Sun and P. J. Stang, Biomedically Relevant Self-Assembled Metallacycles and Metallacages, *J. Am. Chem. Soc.*, 2019, **141**, 14005–14020.
15 S. Rangasamy, H. Ju, S. Um, D. C. Oh and J. M. Song, Mitochondria and DNA Targeting of 5,10,15,20-Tetrakis (7-sulfonatobenzo[b]thiophene) Porphyrin-Induced Photodynamic Therapy via Intrinsic and Extrinsic Apoptotic Cell Death, *J. Med. Chem.*, 2015, **58**, 6864–6874.
16 M. G. Walker, P. J. Jarman, M. R. Gill, X. Tian, H. Ahmad, P. A. Reddy, L. McKenzie, J. A. Weinstein, A. J. Meijer, G. Battaglia, C. G. Smythe and J. A. Thomas, A Self-Assembled Metallomacrocycle Singlet Oxygen Sensitizer for Photodynamic Therapy, *Chem. – Eur. J.*, 2016, **22**, 5996–6000.
17 B. Yuan, J. Liu, R. Guan, C. Jin, L. Ji and H. Chao, Endoplasmic reticulum targeted cyclometalated iridium(III) complexes as efficient photodynamic therapy photosensitizers, *Dalton Trans.*, 2019, **48**, 6408–6415.
18 C. Y. Zhu, M. Pan and C. Y. Su, Metal-Organic Cages for Biomedical Applications, *Isr. J. Chem.*, 2018, **59**, 209–219.
19 K. Li, L. Y. Zhang, C. Yan, S. C. Wei, M. Pan, L. Zhang and C. Y. Su, Stepwise assembly of Pd(6)(RuL(3))(8) nanoscale rhombododecahedral metal-organic cages via metalloligand strategy for guest trapping and protection, *J. Am. Chem. Soc.*, 2014, **136**, 4456–4459.
20 C. Li, Y. Wang, Y. Lu, J. Guo, C. Zhu, H. He, X. Duan, M. Pan and C. Su, An iridium(III)-palladium(II) metal-organic cage for efficient mitochondria-targeted photodynamic therapy, *Chin. Chem. Lett.*, 2020, **31**, 1183–1187.
21 Z. Zhang, Z. Lu, Q. Yuan, C. Zhang and Y. Tang, ROS-Responsive and active targeted drug delivery based on conjugated polymer nanoparticles for synergistic chemo-/photodynamic therapy, *J. Mater. Chem. B*, 2021, **9**, 2240–2248.
22 C. Zhang, K. Wang, X. Guo and Y. Tang, A cationic conjugated polymer with high 808 nm NIR-triggered photothermal conversion for antibacterial treatment, *J. Mater. Chem. C*, 2022, **10**, 2600–2607.
23 S. Chen, K. Li, F. Zhao, L. Zhang, M. Pan, Y. Z. Fan, J. Guo, J. Shi and C. Y. Su, A metal-organic cage incorporating multiple light harvesting and catalytic centres for photochemical hydrogen production, *Nat. Commun.*, 2016, **7**, 13169.
24 Y. P. Wang, K. Wu, M. Pan, K. Li, J. T. Mo, X. H. Duan, H. Z. He, J. Shen and C. Y. Su, One-/Two-Photon Excited Cell Membrane Imaging and Tracking by a Photoactive Nanocage, *ACS Appl. Mater. Interfaces*, 2020, **12**, 35873–35881.
25 W. Lv, Z. Zhang, K. Y. Zhang, H. Yang, S. Liu, A. Xu, S. Guo, Q. Zhao and W. Huang, A Mitochondria-Targeted Photosensitizer Showing Improved Photodynamic Therapy Effects Under Hypoxia, *Angew. Chem., Int. Ed.*, 2016, **55**, 9947–9951.
26 O. Julien and J. A. Wells, Caspases and their substrates, *Cell Death Differ.*, 2017, **24**, 1380–1389.
27 F. C. Machado, R. P. Adum de Matos, F. L. Primo, A. C. Tedesco, P. Rahal and M. F. Calmon, Effect of curcumin-nanoemulsion associated with photodynamic therapy in breast adenocarcinoma cell line, *Bioorg. Med. Chem.*, 2019, **27**, 1882–1890.
28 K. V. Sudheesh, P. S. Jayaram, A. Samanta, K. S. Bejoymohandas, R. S. Jayasree and A. Ajayaghosh, A Cyclometalated Ir(III) Complex as a Lysosome-Targeted Photodynamic Therapeutic Agent for Integrated Imaging and Therapy in Cancer Cells, *Chem. – Eur. J.*, 2018, **24**, 10999–11007.
29 K. Qiu, J. Wang, C. Song, L. Wang, H. Zhu, H. Huang, J. Huang, H. Wang, L. Ji and H. Chao, Crossfire for Two-Photon Photodynamic Therapy with Fluorinated Ruthenium(II) Photosensitizers, *ACS Appl. Mater. Interfaces*, 2017, **9**, 18482–18492.